

Supplement of Atmos. Chem. Phys., 20, 11809–11821, 2020  
<https://doi.org/10.5194/acp-20-11809-2020-supplement>  
© Author(s) 2020. This work is distributed under  
the Creative Commons Attribution 4.0 License.



*Supplement of*

## **Molecular understanding of the suppression of new-particle formation by isoprene**

**Martin Heinritzi et al.**

*Correspondence to:* Joachim Curtius ([curtius@iau.uni-frankfurt.de](mailto:curtius@iau.uni-frankfurt.de))

The copyright of individual parts of the supplement might differ from the CC BY 4.0 License.

## **CLOUD Facility**

We conducted our measurements at the CLOUD (Cosmics Leaving Outdoor Droplets) chamber at CERN (European Center for Nuclear Research), Geneva, Switzerland. The CLOUD chamber is a 26.1 m<sup>3</sup> electro-polished stainless-steel tank used to recreate atmospheric condition in the laboratory (for more details on the chamber see Kirkby et al. (2011); Kirkby et al. (2016); Duplissy et al. (2016)). Data for this study are from the CLOUD 11 and 12 campaigns in autumn 2016 and 2017. Various measures are taken to reduce unwanted contaminants in the CLOUD chamber. The air in the chamber is mixed from cryogenic nitrogen and oxygen, all lines are made of stainless steel and intense cleaning cycles are performed prior to each campaign. Each cleaning cycle consists of at least 24 h of rinsing the chamber from the inside with ultrapure water, followed by a period of at least 24 h with the chamber at 100°C and high ozone levels (several parts per million by volume). These measures result in very low organic contamination below 150 pptv (Kirkby et al., 2016) in total.

Ultrapure water is used to humidify the air in the chamber. Ozone is produced by a UV ozone generator. Liquid  $\alpha$ -pinene (Sigma Aldrich, purity >98 %) is stored in a temperature controlled water bath and evaporated into a dry nitrogen flow and fed into the chamber. Isoprene from a gas bottle (Carbagas AG, purity >99%) is additionally cleaned by a cryotrap. The cryotrap consists of a ~2 m long ¼" stainless steel tube spiral placed in a cryogenic liquid held at 233 K. By using this trap, non-negligible monoterpene-like contaminants in the isoprene gas bottle are effectively frozen out (Bernhammer et al., 2018). Isoprene and  $\alpha$ -pinene are diluted by separate two stage dilution systems prior to being fed into the chamber. All gases are fed into the chamber from the bottom and are mixed by two magnetically driven fans.

A unique feature of the CLOUD chamber is its control of ion concentrations. A high voltage electric field cage ( $\pm 30$  kV) can sweep ions that are constantly produced by naturally occurring galactic cosmic rays out of the chamber in around 1 s. This enables us to study pure neutral nucleation. By switching the field cage off, the naturally formed ions are allowed to stay in the chamber and affect nucleation processes. To artificially enhance ion concentrations, CERN's Proton Synchrotron provides a 3.5 GeV  $\pi^+$  beam that is diverged to >1 m<sup>2</sup> beam profile and crosses the center region of the chamber.

The CLOUD chamber is equipped with four HgXe UV lamps (LightningCure LC8, Hamamatsu Photonics K.K.) positioned at the top of the chamber and connected via fiber bundles. An additional UV source is provided by a KrF excimer laser (ATLEX-1000, ATL Lasertechnik GmbH) at 248 nm wavelength and also connected to the chamber via fiber bundles to enhance OH $\cdot$  production via photolysis of O<sub>3</sub> further.

## **Typical Run sequence and conditions**

Our experiments were performed at +5 and +25 °C and mostly 38 % relative humidity. A typical run sequence can be seen in Fig. S1 and S2. First,  $\alpha$ -pinene is present with ozone under both neutral and ger conditions at three different atmospherically relevant concentrations. HOMs are forming as seen by the CI-API-TOF and new-particle formation is induced. The purpose of this experiment was also to ensure inter-campaign comparability to Kirkby et al. (2016). In the following run a stable isoprene concentration is established in the chamber and ozone is added shortly afterwards. As ozone and isoprene only react very slowly, effects on HOMs are minor. As UV light in the chamber is switched on, OH $\cdot$  production increases and thus formation of OH $\cdot$  induced isoprene HOMs. However, only the subsequent addition of  $\alpha$ -pinene leads to formation of C<sub>20</sub> class HOMs and thus new-particle formation. UV effects were studied by switching on the Hamamatsu lamp, as well as the KrF-excimer laser.

## **Gas-phase measurements**

Ozone was measured by a calibrated ozone monitor (Thermo Environmental Instruments TEI 49C). Isoprene and  $\alpha$ -pinene were measured by the newly developed proton transfer reaction time-of-flight mass spectrometer (PTR3 (Breitenlechner et al., 2017)). The instrument was frequently calibrated for both gases

and has a limit of detection of 2 pptv for isoprene and  $\alpha$ -pinene for 1 s integration time. The accuracy of the instrument for both gases is mainly determined by the uncertainty of the calibration gas standard (5 %) and accuracies of mass flow controllers and is estimated to be 7 %.

The chemical ionization atmospheric pressure interface time-of-flight (CI-APi-TOF) mass spectrometer (Tofwerk AG) measured highly-oxygenated organic compounds with a limit of detection of  $\sim 5 \cdot 10^4 \text{ cm}^{-3}$ . The instrument operates with a nitrate based ion source similar to the design in Eisele and Tanner (1993). However, a corona discharge was used instead of a radioactive source (Kürten et al., 2011). The instrument was calibrated for sulfuric acid (Kürten et al., 2012) and the data corrected for mass dependent transmission efficiency (Heinritzi et al., 2016). HOM quantification was performed as described in Kirkby et al. (2016). The run-to-run uncertainty for HOMs is estimated to be 20 %. Due to technical reasons at the start of CLOUD 11 the CI-APi-TOF could only start measuring at 03 Oct 2016, 10:28 UTC (see Fig. S1). As HOMs depend linearly on the product [ $\alpha$ -pinene] $\cdot$ [O<sub>3</sub>] (Kirkby et al., 2016; Ehn et al., 2014), HOM concentrations measured during the mid  $\alpha$ -pinene settings were used and scaled down according to this relation to obtain HOM concentrations for the low  $\alpha$ -pinene settings for the appropriate times where  $J$  and growth rates were estimated. This also gave a higher uncertainty for this data point (28 %) as indicated in Fig. 3A. The overall uncertainty in HOM quantification consists of contributions from sulfuric acid calibration (+50 %/-33 %), charging efficiency of HOMs in the ion source (25 %), transmission correction (50 %) and sampling line loss correction (20 %). This results in an overall scale uncertainty for HOMs of +78 %/-68 %. There are however additional uncertainties in our HOM estimation that cannot be readily quantified. On the one hand nitrate ionization of HOMs shows a drop in charging efficiency for HOMs with six or less oxygen atoms (Hytinen et al., 2017). This leads to an underestimation of these molecules. However, these molecules with comparably low oxygen content are not expected to contribute significantly to nucleation and early growth. Additionally, it was shown that nitrate ionization has a reduced charging efficiency towards HOMs formed by OH $\cdot$  oxidation compared to HOMs formed by ozonolysis (Berndt et al., 2015; Berndt et al., 2016). This could affect also C<sub>20</sub> class molecules that show OH $\cdot$  dependence, like C<sub>20</sub>H<sub>32</sub>O<sub>7</sub> (see Figure S1). The real increase of these C<sub>20</sub> class HOMs due to UV light could be larger than the measured one, thus dampening the overall decrease of C<sub>20</sub> when UV is switched on. The fact that  $J$  decreases when UV is switched on, however, confirms that the total nucleating molecules in the chamber decrease. That effect is thus not strong enough to lead to a real increase instead of a decrease in C<sub>20</sub> class molecules.

We group all HOMs within the  $m/z$  range from 235 to 625 Th in four groups according to their carbon number. This  $m/z$  range was chosen to remain consistent with the definition of total HOM in Kirkby et al. (2016). We sum up HOMs with 2-5, 6-10, 11-15 and 16-20 carbon atoms to get C<sub>5</sub>, C<sub>10</sub>, C<sub>15</sub> and C<sub>20</sub> class HOMs, respectively. The sum of these four classes represents HOM total as shown e.g. in Fig. 3.

### OH $\cdot$ estimation and comparison to ambient environments

We estimate OH $\cdot$  levels in our chamber via a steady state approach (see Fig. S1). OH $\cdot$  sources taken into account are ozonolysis of  $\alpha$ -pinene and isoprene, with yields of 79 % (Tillmann et al., 2010) and 26 % (Malkin et al., 2010; Kroll Jesse et al., 2001), respectively, as well as photolysis of ozone with our UV laser. The OH $\cdot$  source strength of the UV laser was characterized with a separate experiment (SO<sub>2</sub> to sulfuric acid conversion) and depends on laser settings, ozone concentration and absolute water vapor concentration. Sink terms taken into account are reactions of OH $\cdot$  with  $\alpha$ -pinene and isoprene. Secondary reactions of OH $\cdot$  with further oxidation products of  $\alpha$ -pinene or isoprene are not taken into account, as their effect is expected to be minor (e.g. two orders of magnitude smaller than the former sink terms in case of the pinonaldehyde-OH $\cdot$  reaction). OH $\cdot$  recycling in our chamber is expected to be weak, as we do not have NO<sub>x</sub> in the chamber and many runs are performed under dark conditions. The recycling mechanism due to photolysis of hydroperoxy-aldehydes (HPALDs) (Taraborrelli et al., 2012) can in principal take place during UV runs, however, HPALDs may also decompose on our stainless steel chamber walls without releasing OH $\cdot$  in a process similar to the one described in Bernhammer et al. (2017), thus further reducing recycling efficiency. However, the O<sub>x</sub> recycling mechanisms (reaction of O<sub>3</sub> and HO<sub>2</sub> yielding OH $\cdot$ , as well as photolysis of H<sub>2</sub>O<sub>2</sub> under UV conditions) might take place in our conditions (Lelieveld et al., 2016). All gas phase reaction rate constants are preferred values provided by IUPAC (International Union of Pure and

Applied Chemistry) and were evaluated at +5 °C ( $k_{\text{apO}_3} = 8.1 \cdot 10^{-17} \text{ cm}^3 \text{ s}^{-1}$ ,  $k_{\text{apOH}} = 5.8 \cdot 10^{-11} \text{ cm}^3 \text{ s}^{-1}$ ,  $k_{\text{ipO}_3} = 7.9 \cdot 10^{-18} \text{ cm}^3 \text{ s}^{-1}$  and  $k_{\text{ipOH}} = 1.1 \cdot 10^{-10} \text{ cm}^3 \text{ s}^{-1}$ ) and +25 °C ( $k_{\text{apO}_3} = 9.4 \cdot 10^{-17} \text{ cm}^3 \text{ s}^{-1}$ ,  $k_{\text{apOH}} = 5.2 \cdot 10^{-11} \text{ cm}^3 \text{ s}^{-1}$ ,  $k_{\text{ipO}_3} = 1.3 \cdot 10^{-17} \text{ cm}^3 \text{ s}^{-1}$  and  $k_{\text{ipOH}} = 1.0 \cdot 10^{-10} \text{ cm}^3 \text{ s}^{-1}$ ).

We calculate OH· levels of around  $1 \cdot 10^6 \text{ cm}^{-3}$  during dark  $\alpha$ -pinene ozonolysis, with roughly a doubling to  $2 \cdot 10^6 \text{ cm}^{-3}$  when the UV laser is switched on. When isoprene is present together with  $\alpha$ -pinene it foremost acts as a sink for OH· and thus reduces its concentrations. The strength of this depletion depends on the main OH· source strength, i.e., the  $\alpha$ -pinene ozonolysis rate. We find OH· levels 5 to 20 times lower when isoprene is present than under  $\alpha$ -pinene only conditions. This depletion can also be recognized in the traces of HOMs that originate from OH· oxidation, like  $\text{C}_{10}\text{H}_{18}\text{O}_6$  (see Fig. S1).

In the atmosphere, OH· levels of  $10^6 \text{ cm}^{-3}$  and higher are reported even in the presence of isoprene, as several OH· recycling mechanisms take place (Lee et al., 2016; Martinez et al., 2010; Lelieveld et al., 2016). However, given the reduction in  $\text{C}_{20}$  class molecules when OH· is increased from  $2 \cdot 10^5 \text{ cm}^{-3}$  to  $4 \cdot 10^5 \text{ cm}^{-3}$  by switching on UV light, it is a reasonable assumption that, if OH· would be fully replenished to  $1 \cdot 10^6 \text{ cm}^{-3}$ , we would see a further decrease of total  $\text{C}_{20}$  class molecules and subsequently a reduction in  $J$  and early growth rates. This assumption is also valid when the reduced charging efficiency of nitrate ionization towards OH· initiated HOMs is taken into account as outlined above. The decrease of  $\text{C}_{20}$  class molecules and nucleation rate when OH· is increased is direct evidence that the suppression effect of isoprene on nucleation is not due to depletion of OH·.

## Particle Measurements

The total particle number concentration above 2.5 nm is measured by a TSI 3776 condensation particle counter (CPC) using butanol as working fluid. For smaller particles, an Airmodus A10 particle size magnifier (PSM), using diethylene glycol as working fluid, is used (Vanhanen et al., 2011) in combination with an Airmodus A20 CPC. This setup achieves detection of airborne particles down to 1 nm. By varying the supersaturation inside the PSM, particle size distributions between 1 – 3 nm can be inferred (Lehtipalo et al., 2014).

A DMA-train (Stolzenburg et al., 2017) is used to measure the particle size distribution and growth rates between 1.8 – 8.0 nm. It uses a parallel design of six sampling channels each equipped with a differential mobility analyser (DMA) together with an ultrafine condensation particle counter (uCPC). For detection of sub-2.5 nm particles, two of the channels are equipped with either an Airmodus A10 particle size magnifier (PSM) or a TSI 3777 nanoEnhancer as booster stage upstream of the CPC. The channels are operated at fixed sizes to increase time-resolution and counting-statistics leading to higher sensitivities for smaller sizes compared to standard scanning mobility devices.

The size distribution above 5 nm is measured with a TSI Scanning Mobility Particle Sizer (nanoSMPS, Model 3938) using a TSI 3082 nanoDMA and a water-based TSI 3788 CPC for detection of the size-selected particles. For particles larger than 65 nm a custom-built SMPS with a long column DMA was used.

## Determination of nucleation rates

The nucleation rate  $J$  defines the number of particles formed within a volume per unit of time. It is calculated using the flux of the total concentration of particles growing past a specific diameter (here at 1.7, 2.2, 2.5 and 6 nm). In the following, the method for calculating  $J_{1.7}$  is presented, however the calculation for  $J_{2.2}$ ,  $J_{2.5}$  and  $J_6$  follows the same procedure unless specified otherwise. The nucleation rate is the sum of the

time derivative of the concentration of particles above a certain diameter, as well as correction terms accounting for aerosol losses due to dilution in the chamber, wall losses and coagulation.

$$J_{1.7} = \frac{dN_{\geq 1.7 \text{ nm}}}{dt} + S_{dil} + S_{wall} + S_{coag} \quad (1)$$

$N$  is the concentration of particles of diameter equal or larger than 1.7 nm. The term  $S_{dil}$  describes the size-independent losses of particles due to dilution of the gases in the chamber. The chamber is continuously flushed with a total flow of 230 liters per minute to replenish the sampling flow of the instruments. This results in the dilution factor  $k_{dil} = 1.47 \cdot 10^{-4} \text{ s}^{-1}$  and

$$S_{dil} = N_{\geq 1.7 \text{ nm}} \cdot k_{dil} \quad (2)$$

The term  $S_{wall}$  describes the size-dependent particle losses to the chamber walls and was calculated based on the decay rate of sulfuric acid monomer (of mobility diameter = 0.85 nm (Kulmala et al., 2013)) in the chamber (at temperature = 278 K). The wall loss rate  $k_{wall}$  is a function of particle diameter and temperature.

$$S_{wall}(T) = \sum_{d_{p,i}=1.7 \text{ nm}}^{d_{p,max}} N(d_{p,i}) \cdot k_{wall}(d_{p,i}, T) \quad (3)$$

At 278 K

$$k_{wall}(d_{p,i}) = 1.7 \cdot 10^{-3} \text{ nm s}^{-1} \cdot \frac{1}{d_{p,i}} \quad (4)$$

The term  $S_{coag}$  represents the coagulation losses to the surface of pre-existing aerosol particles in the chamber and was calculated using the full number size distribution present in the chamber (Seinfeld and Pandis, 2016).

$$S_{Coag}(d_p = 1.7 \text{ nm}) = \sum_{d_{p,i}=d_p}^{d_{p,max}} \sum_{d_{p,j}=d_p}^{d_{p,max}} \delta_{i,j} \cdot K(d_{p,i}, d_{p,j}) \cdot N_i \cdot N_j \quad (5)$$

where  $K(d_{p,i}, d_{p,j})$  is the coagulation coefficient for particles of the size  $d_{p,i}$  and  $d_{p,j}$ ,  $N_i$  and  $N_j$  are the number concentrations of particles in the size bins  $d_{p,i}$  and  $d_{p,j}$ , and  $\delta_{i,j} = 0.5$ , if  $i = j$  and  $\delta_{i,j} = 1$ , if  $i \neq j$ .  $d_{p,i}$  is the midpoint diameter for the size bin with index  $i$ .

The number size distribution of particles used for the calculation of formation rates were obtained from the scanning PSM at cut-off diameters 1.7 nm and 2.2 nm for the determination of  $J_{1.7}$  and  $J_{2.2}$ , and from a butanol CPC (model CPC3776, TSI Inc.) of fixed cut-off (2.5 nm) for determining the formation rate of 2.5 nm particles. For determining  $J_6$  the integrated size bins from the nanoSMPS were used. A correction factor of +0.3 nm on the cut-off diameter of the PSM was included to account for the poorer detection efficiency of neutral organic particles compared to calibration with tungsten oxide (Kangasluoma et al., 2014). The concentrations obtained were corrected for sampling line losses. During each run, the value of  $J$  was determined after reaching a steady state value. A median value of the formation rate was then obtained. The errors on the reported  $J$  rates were obtained by considering an inter-campaign reproducibility error of 30 % as well as a series of run-dependent systematic and statistical uncertainties which include errors on sampling (10 %), dilution (10 %), wall loss (20 %) and coagulation sink (20 %). The resulting overall scale uncertainty for  $J$  is 47 %.

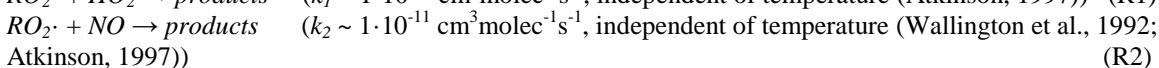
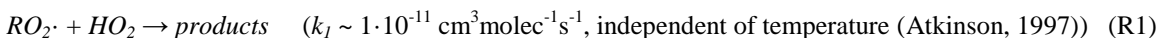
### Determination of growth rates

Particle growth rates were derived from several instruments individually with the widely used appearance time method (Lehtipalo et al., 2014). For this method the signal rise in a single size channel is fitted with a sigmoidal function during the particle formation event. The fit determines the appearance time  $t_{app}$  at which

the signal intensity reaches 50 % between a potential background and the final value reached at steady-state nucleation conditions. A linear fit of  $t_{app}$  and the corresponding diameters of several size channels yields an average apparent growth rate of the size distribution for a diameter interval. To infer a size-dependence of the measured growth rates, several instruments and size-intervals were used. Growth rates between 1.3 – 1.9 nm were measured with the scanning PSM, the DMA-train size channels were split up into two intervals, one between 1.8 – 3.2 nm and one between 3.2 – 8.0 nm. For size-intervals above 8 nm the size channels of the nanoSMPS was used. Uncertainties in the sigmoidal fit result are promoted to the linear fit of the growth rate providing an estimate of the statistical uncertainties. However, at least a systematic uncertainty of approximately 50 % has to be assumed if apparent growth rates are interpreted as condensational growth values.

### Effect of lighter VOCs on RO<sub>2</sub>· chemistry and HOM formation

Organic peroxy radical (RO<sub>2</sub>·) branching is critical to atmospheric chemistry. There are many thousands of different RO<sub>2</sub>· radicals, but their chemistry can be simplified to the following basic reaction set:



This neglects important exceptions such as peroxy acyl radicals reacting with NO<sub>2</sub> to form PANs, but is sufficient to describe the essential features here and in the atmosphere (Finlayson-Pitts and Pitts Jr, 1999). The maximum rate constant (the collision constant) is roughly  $3 \cdot 10^{-10} \text{ cm}^3 \text{ molec}^{-1} \text{ s}^{-1}$ , so R1 and R2 occur at slightly under one in ten collisions with only a very modest temperature dependence. Experimental kinetics show that the rate constants for these first two reactions depend only weakly on the organic substituent R (Finlayson-Pitts and Pitts Jr, 1999), and so here we consider two similar, temperature independent rate constants for all RO<sub>2</sub>·.

The ubiquity and similarity of the first two rate constants means that “high-NO<sub>x</sub>” chemistry is well defined. The ratio of NO to HO<sub>2</sub> is crucial. Data show that typical daytime HO<sub>2</sub> is around 2 – 30 pptv (Elshorbany et al., 2012; Stevens et al., 1997; Lelieveld et al., 2016; Finlayson-Pitts and Pitts Jr, 1999) (with photolysis of aldehydes, especially formaldehyde and oxidation of CO by OH being drivers of HO<sub>2</sub> concentrations (Finlayson-Pitts and Pitts Jr, 1999; Lelieveld et al., 2016)) and so if [NO] is larger than these values the reaction with NO will outcompete the reaction with HO<sub>2</sub> and the system becomes “high NO<sub>x</sub>”. However, even under “low NO<sub>x</sub>” conditions, high HO<sub>2</sub> levels can also reduce nucleation and early growth, as R1 only forms C<sub>10</sub> monomers and no C<sub>20</sub> dimers for monoterpene oxidation.

The total [RO<sub>2</sub>] in the atmosphere rarely exceeds [HO<sub>2</sub>] and is often significantly lower. Further, unlike the first two reactions, the RO<sub>2</sub> + RO<sub>2</sub> reactions depend strongly on the organic substituent, varying by over six orders of magnitude at room temperature (Madronich and Calvert, 1990). In general, electron donating substituents (i.e. t-butyl) make the reaction very slow, while electron withdrawing substituents (i.e. acetyl) can make the self-reaction fairly fast (CH<sub>3</sub>C(O)O<sub>2</sub> + CH<sub>3</sub>C(O)O<sub>2</sub>  $\sim 1 \cdot 10^{-11} \text{ cm}^3 \text{ molec}^{-1} \text{ s}^{-1}$ ) (Madronich and Calvert, 1990). Madronich and Calvert (1990) proposed a simplifying scheme to estimate cross reaction rate constants from self-reaction rate constants using the geometric mean ( $k_{a,b,cross} = 2 \cdot \sqrt{k_{a,self} \cdot k_{b,self}}$ ). Recently, it was shown (Berndt et al., 2018) that highly oxidized RO<sub>2</sub>· produced from terpenes such as α-pinene can have  $k_3 \sim 1 \cdot 10^{-10} \text{ cm}^3 \text{ molec}^{-1} \text{ s}^{-1}$ .

These rapid RO<sub>2</sub>· + RO<sub>2</sub>· reactions are extremely important for atmospheric chemistry and the analysis we present here. Only when  $k_3 \gg 1 \cdot 10^{-11} \text{ cm}^3 \text{ molec}^{-1} \text{ s}^{-1}$ , can RO<sub>2</sub>· cross reactions have a significant effect in the atmosphere, but when this is true there are two consequences. First, the oxidation mechanisms of different hydrocarbons producing highly reactive RO<sub>2</sub>· become coupled, because they influence each other through their RO<sub>2</sub>·. Second, the transition to “high NO<sub>x</sub>” is pushed to higher NO because of the faster self-reactions.

It is the first consequence that is most significant here. The  $\text{RO}_2\cdot$  from  $\alpha$ -pinene and isoprene both appear to be highly reactive and so will out compete  $\text{HO}_2$  at low NO. Consequently, isoprene and monoterpenes become coupled by their  $\text{RO}_2\cdot$  interactions.  $\text{RO}_2\cdot$  radicals derived from smaller VOCs like  $\text{CH}_4$  can have significantly lower self-reaction rates (e.g. for  $\text{CH}_3\text{OO}\cdot$   $k_{\text{self}} = 3.5 \cdot 10^{-13} \text{ cm}^3 \text{ molec}^{-1} \text{ s}^{-1}$ ) (Madronich and Calvert, 1990). The resulting cross reaction would then be  $1.2 \cdot 10^{-11} \text{ cm}^3 \text{ molec}^{-1} \text{ s}^{-1}$  and thus one order of magnitude smaller than the  $\text{RO}_2(\alpha\text{p})$  self-reaction rate. This would allow for at least some degree of coupling, depending on detailed atmospheric conditions.

However, if  $\text{RO}_2\cdot$  coupling of light VOCs or  $\text{HO}_2$  would dominate atmospheric chemistry of  $\text{RO}_2(\alpha\text{p})$ , it would not be possible to detect C20 signals there, as almost all  $\text{RO}_2(\alpha\text{p})$  radicals would be terminated to either C10 monomers or light dimers with e.g. 11 or 12 carbon atoms. There is however clear evidence of atmospheric C20 formation, i.e.  $\text{RO}_2(\alpha\text{p})$ - $\text{RO}_2(\alpha\text{p})$  reactions leading to dimers in the presence of relatively high levels of CO,  $\text{CH}_4$ ,  $\text{HO}_2$  and in some locations also NO<sub>x</sub> (Yan et al., 2016; Kürten et al., 2016; Massoli et al., 2018). The HOM spectrum reported for an isoprene-rich measurement site in Alabama during the SOAS campaign showed a qualitatively similar distribution of C5, C10, C15 and C20 classes as reported in our study (except for NO<sub>x</sub> effects) (Massoli et al., 2018). This is direct evidence for the atmospheric relevance of our findings.

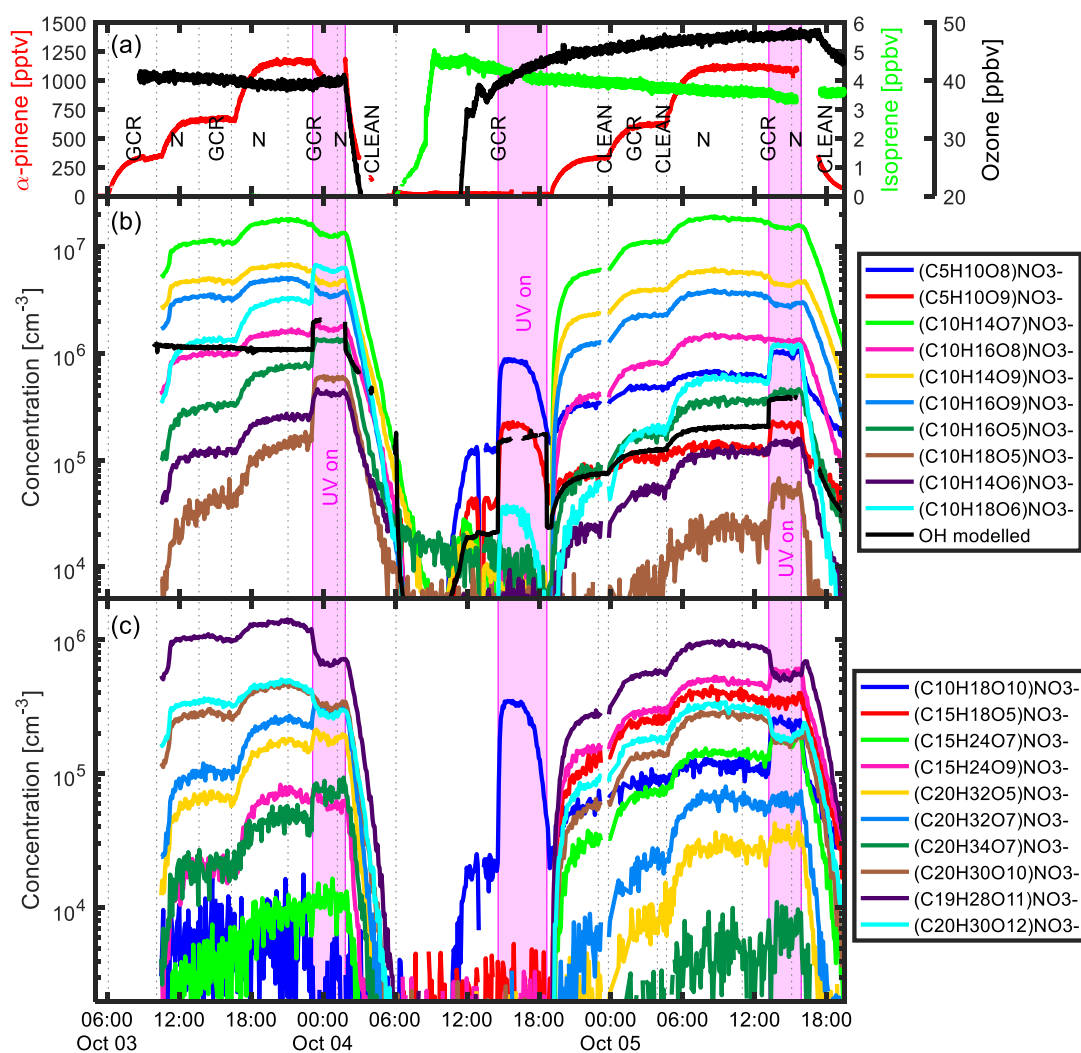


**Figure S1: Time series of a nucleation experiment with example HOM traces.** (a) shows traces of  $\alpha$ -pinene, isoprene and ozone. (b) and (c) show selected time traces of HOM monomers and dimers measured by the CI-API-TOF, respectively. The temperature in the chamber was +5 °C and rel. humidity was 38 %. N, GCR and CLEAN indicate neutral (high voltage cleaning field on), galactic cosmic ray (high voltage cleaning field off) and cleaning (neutral periods to clean the chamber of particles) conditions, respectively. In the first part until 04 Oct, 06:00 UTC,  $\alpha$ -pinene was present in the chamber at three different concentrations to study pure biogenic nucleation under both neutral and gcr conditions with an additional UV stage at the end. Afterwards an isoprene/ozone mixture was studied under both dark and UV-illuminated conditions. Note that during the UV stage on 04 Oct the laser intensity deteriorated towards the end of the stage and thus corresponding HOM signals went down as well. At 04 Oct, starting at 18:40 UTC,  $\alpha$ -pinene was added at three concentration levels similar to the first part of the experiment.

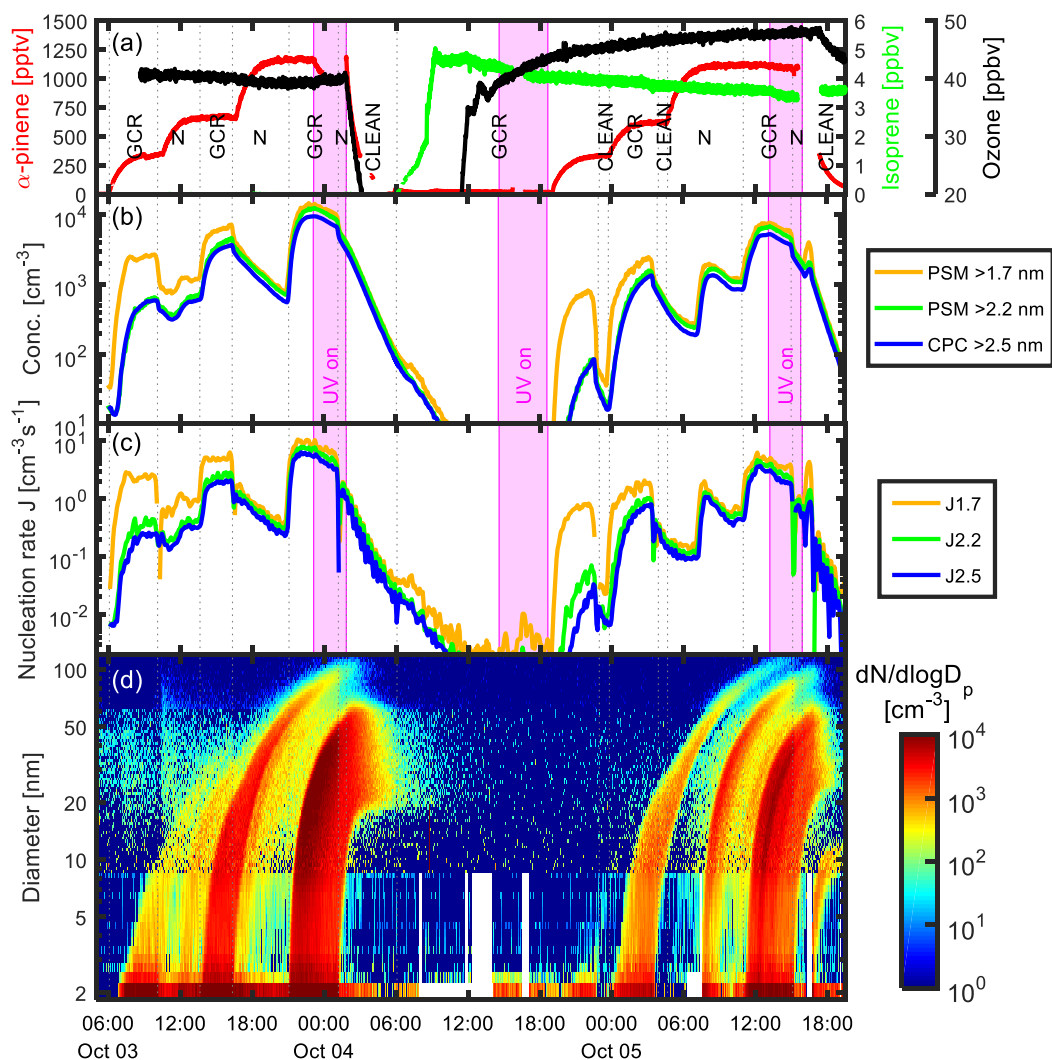


**Figure S2: Time series of a nucleation experiment with particle counter data and nucleation rates.** The temperature in the chamber was +5 °C and rel. humidity was 38 %. The time window shown is the same as in Figure S1. **(a)** shows traces of  $\alpha$ -pinene, isoprene and ozone. N, GCR and CLEAN indicate neutral (high voltage cleaning field on), galactic cosmic ray (high voltage cleaning field off) and cleaning (neutral periods to clean the chamber of particles) conditions, respectively. **(b)** shows particle concentration above 1.7, 2.2 and 2.5 nm, measured with a scanning PSM (1.7 nm and 2.2 nm) and a butanol-based CPC (2.5 nm). **(c)** shows the nucleation rate  $J$  determined at 1.7, 2.2 and 2.5 nm using the particle concentrations shown in (b). **(d)** shows a combined size distribution of aerosol particles in the CLOUD chamber. The DMA-train contributed the size range from 1.8 – 8 nm, the nanoSMPS from 8 – 65 nm and the long-SMPS for sizes >65 nm.

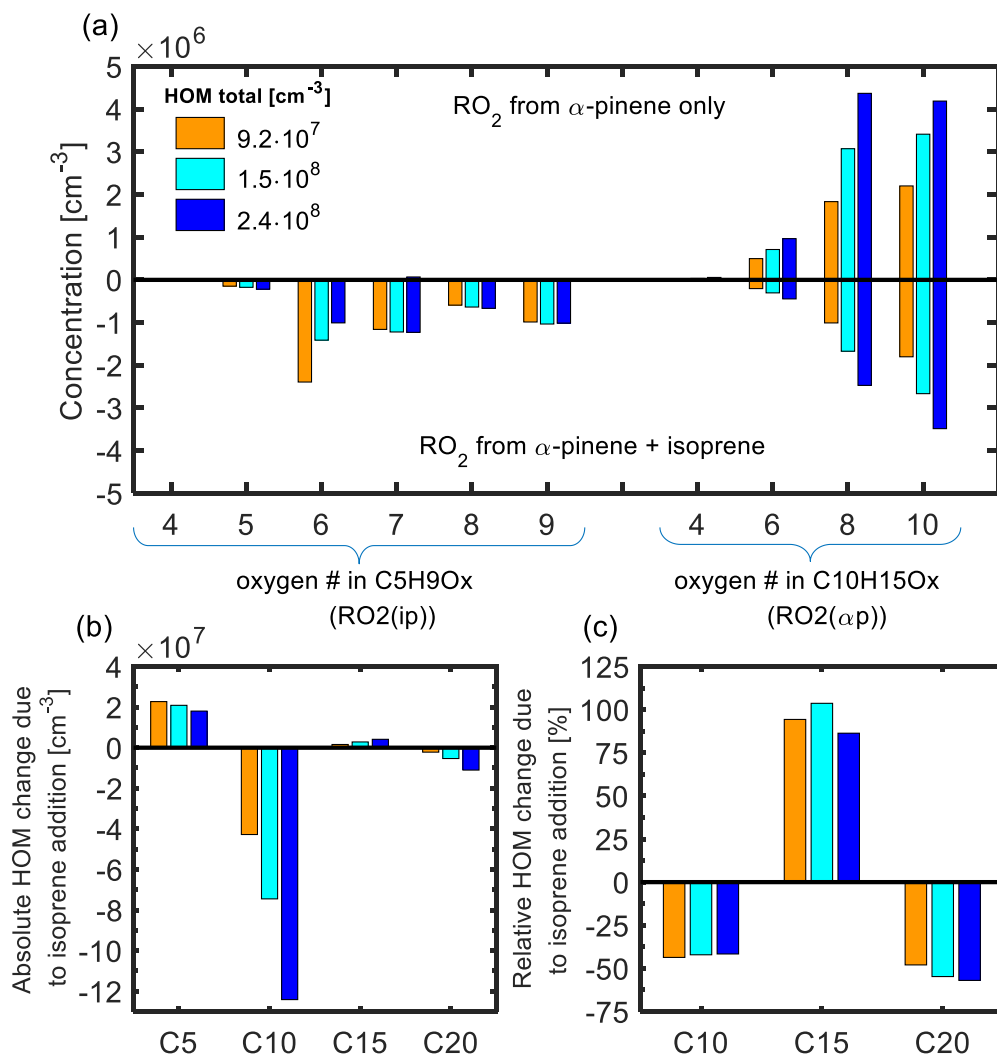


**Figure S3: Effects of isoprene addition on RO<sub>2</sub>· radical and HOM classes distribution.** Chamber conditions were +25 °C and 38 % RH. α-Pinene levels were 456, 771 and 1442 pptv for α-pinene only and 677, 1326 and 2636 pptv for α-pinene + isoprene conditions. Ozone levels were 49 ppbv for α-pinene only and 38 to 40 ppbv for α-pinene + isoprene conditions. Isoprene levels were 2.7, 4.9 and 9.8 ppbv. All data from the α-pinene only runs was scaled up linearly (21, 38 and 45 % for low, mid and high α-pinene levels, respectively) to match the exact same [α-pinene] · [O<sub>3</sub>] values as in the α-pinene + isoprene runs. **(a)** shows the distribution of the most prominent RO<sub>2</sub>· radicals originating from isoprene and α-pinene oxidation. **(b)** shows the absolute and **(c)** the relative changes of the HOM class distribution due to isoprene addition.

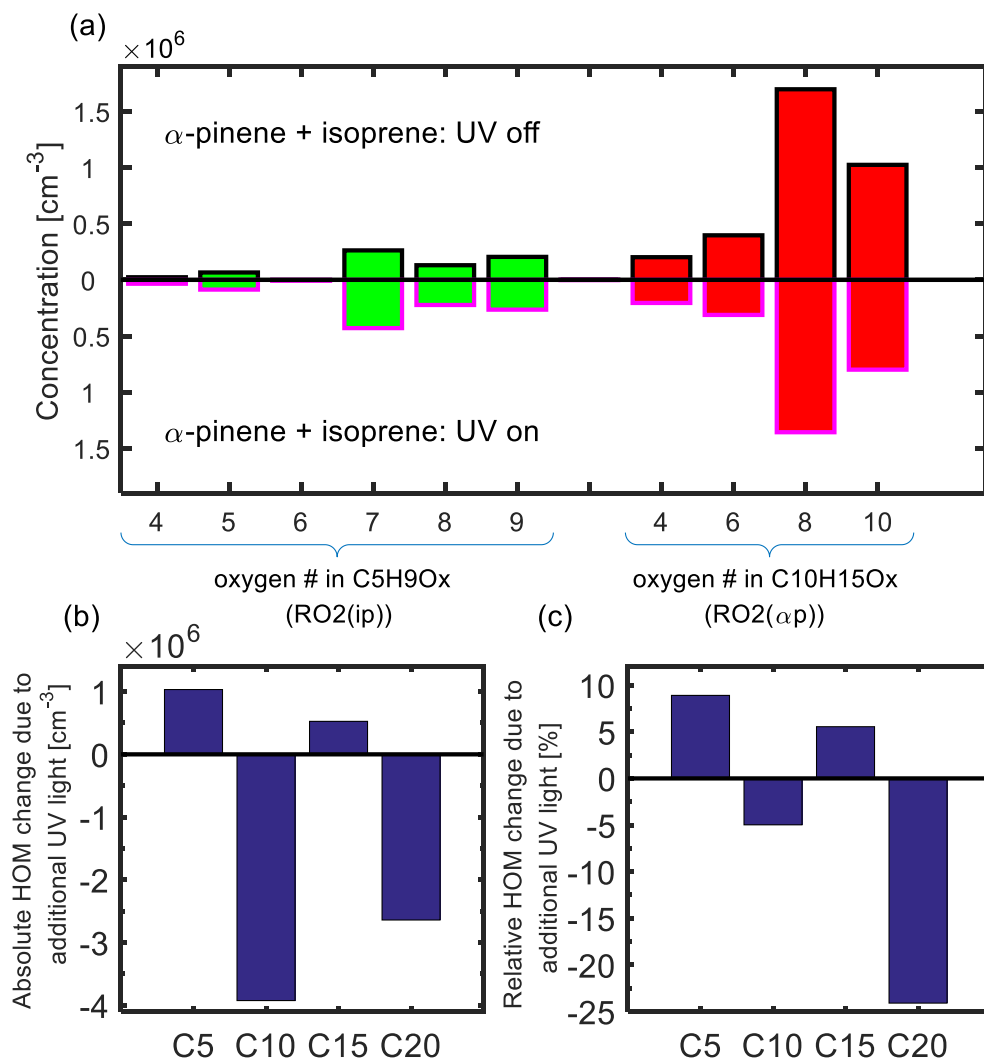


**Figure S4: Changes of  $\text{RO}_2\cdot$  radical and HOM classes distribution due to UV light in an  $\alpha$ -pinene, isoprene and ozone mixture.** Chamber conditions were  $+5\text{ }^\circ\text{C}$  and 38 % RH.  $\alpha$ -pinene levels were 1116 (dark) and 1096 pptv (UV illuminated). The ozone level was 48 ppbv, the isoprene level was 3.6 and 3.4 ppbv in dark and UV illuminated conditions, respectively. Data from the dark run was slightly scaled down linearly (1.2 %) to match exact same  $[\alpha\text{-pinene}] \cdot [\text{O}_3]$  values as in the UV run. **(a)** shows the distribution of the most prominent  $\text{RO}_2\cdot$  radicals originating from isoprene (green) and  $\alpha$ -pinene (red) oxidation. **(b)** shows the absolute and **(c)** the relative changes of the HOM class distribution due to UV light.

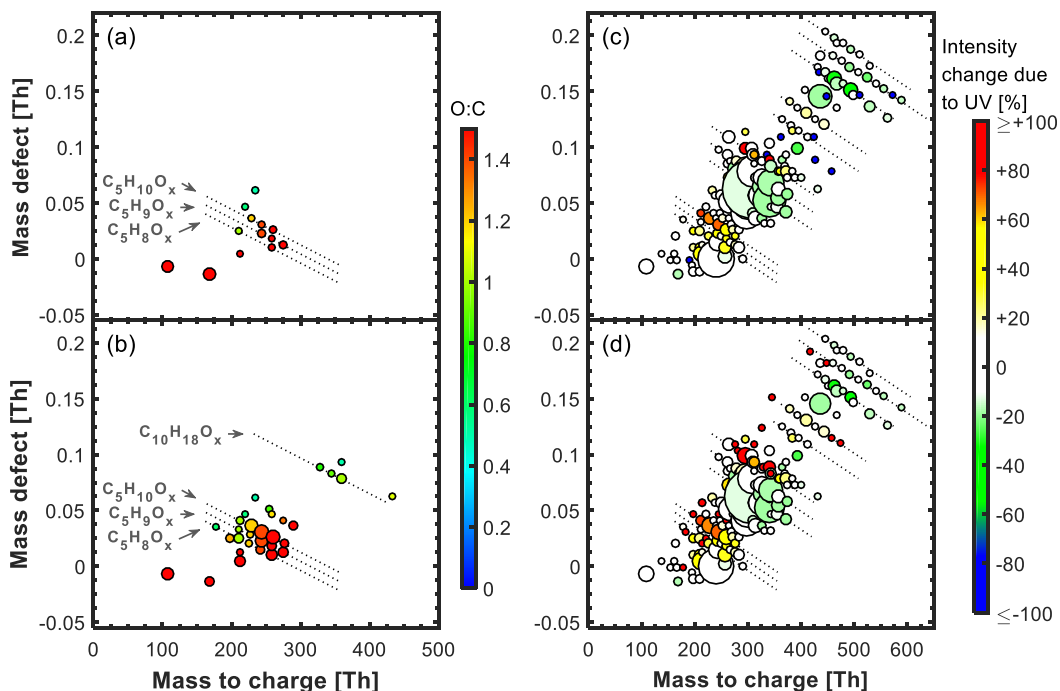


**Figure S5: Mass defect plots showing HOM production from isoprene alone (a, b) and the effect of UV light on an  $\alpha$ -pinene/isoprene mixture (c, d).** Chamber conditions were +5 °C and 38 % RH. HOM production from a mixture of isoprene (4.5 ppbv) and ozone (40 – 50 ppbv) under (a) dark conditions and (b) UV-illuminated conditions with higher OH $\cdot$  levels. The area of the marker points is linearly scaled to intensity of the HOM signals in all four panels. Color code represents oxygen-to-carbon ratio (O:C) of HOMs. UV light strongly enhances OH $\cdot$  and thus HOM production. This even leads to the formation of some C<sub>10</sub> dimers resulting from the combination of two RO<sub>2</sub>(ip). (c) and (d) show the mass defect plot of HOMs from a mixture of  $\alpha$ -pinene, isoprene and ozone under (c) dark and (d) UV-illuminated conditions.  $\alpha$ -pinene is 1116 and 1096 pptv, isoprene was 3.6 and 3.4 ppbv in (c), and (d), respectively. Ozone was 47 ppbv for both runs. Color code indicates the change in intensity for each HOM peak when switching from dark to UV light conditions, i.e. the percentage intensity change between (c) and (d). The color for each peak is thus the same in (c) and (d). Data from the dark run was slightly scaled down linearly (1.2 %) to match the same [ $\alpha$ -pinene]·[O<sub>3</sub>] values as in the UV run for calculating the intensity change.

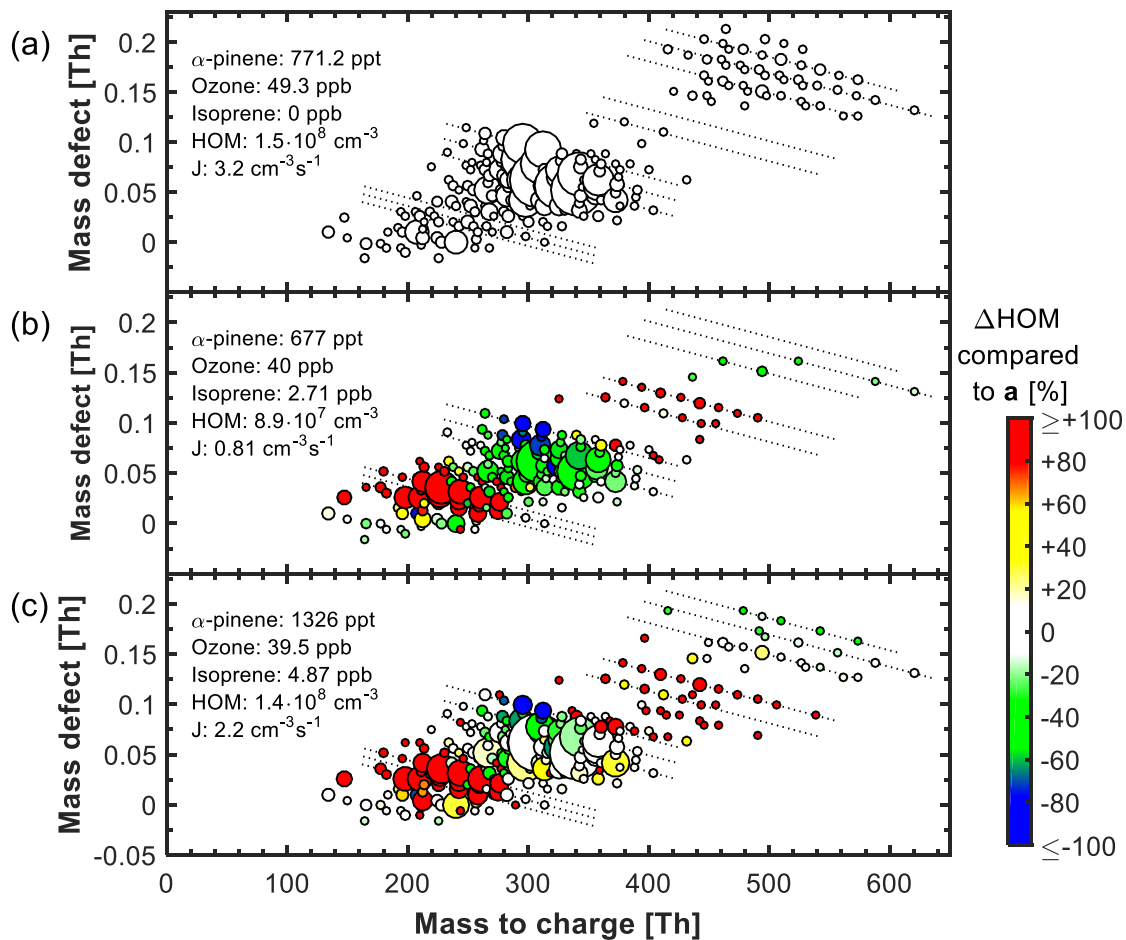


**Figure S6: Mass Defect plots showing the effect of increased isoprene and monoterpene concentrations on HOM formation and nucleation rate  $J_{1,7}$ .** Chamber conditions were +25 °C and 38 % RH. (a) describes the base case without isoprene, (b) shows the effect of addition of isoprene. Color code in (b) and (c) shows the relative change in HOM intensity compared to (a). (c) shows HOM spectra after  $\alpha$ -pinene and isoprene concentrations have been roughly doubled compared to (b).

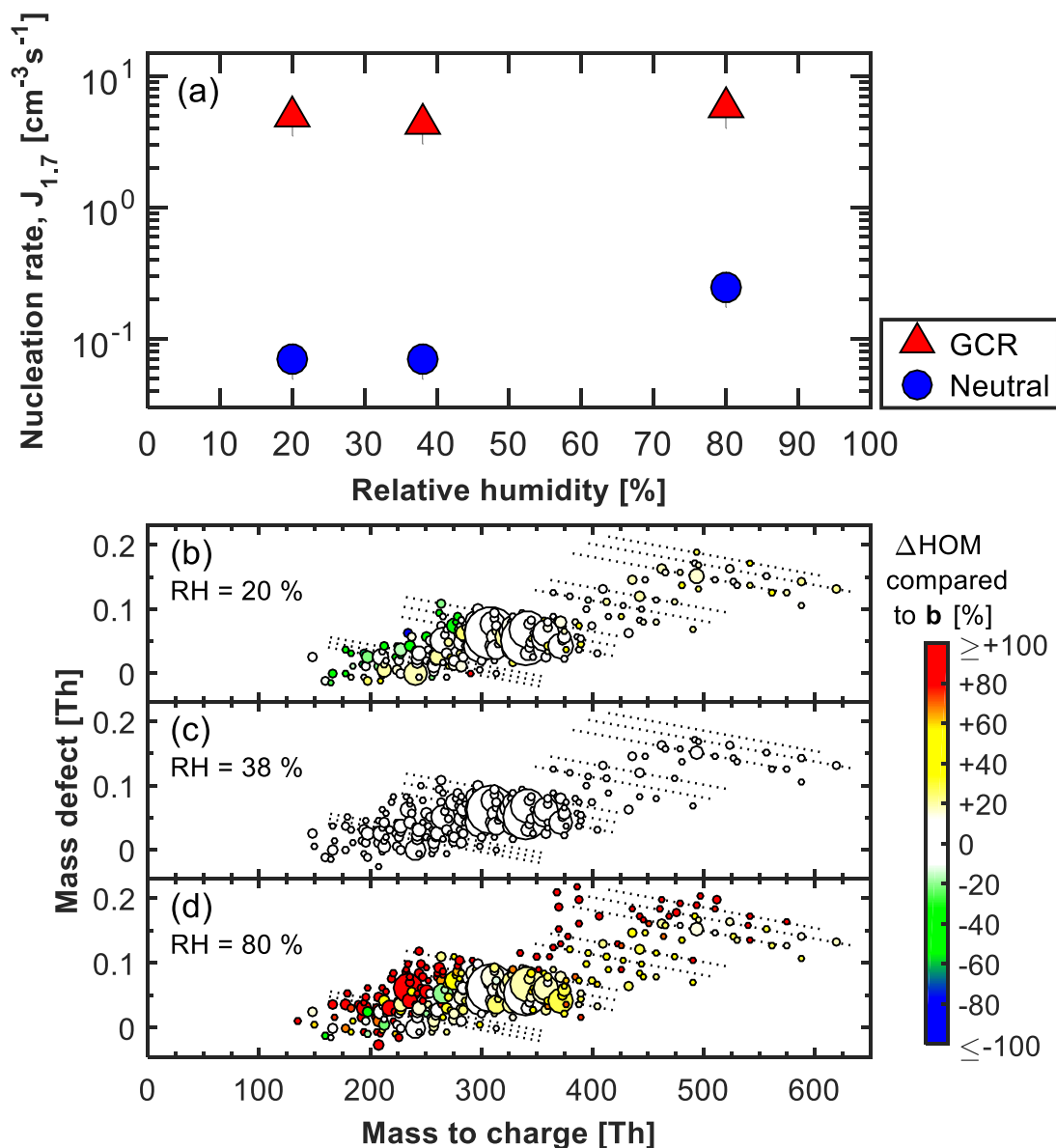


**Figure S7: Nucleation rate  $J_{1,7}$  vs relative humidity at +25 °C (a) and corresponding HOM spectra (b-d).** All data shown was recorded with similar precursor concentrations (1.4 ppbv  $\alpha$ -pinene, 5.1-6.2 ppbv isoprene, however, ozone decreased slightly from 46 to 40 ppbv as humidity was increased). HOM levels were fairly constant ranging from  $1.3 \cdot 10^8$  to  $1.6 \cdot 10^8 \text{ cm}^{-3}$ . Bars indicate  $1\sigma$  run-to-run uncertainty. The overall systematic scale uncertainty of  $J$  for  $\pm 47\%$  is not shown. The mass defect plots (b, c and d) show the HOM distribution measured by the nitrate CI-API-TOF under different humidity levels. The color code represents the relative change in HOM signal compared to the standard 38 % RH setting shown in (c). To calculate this change, HOM levels in (b) and (d) were scaled down by 11 % and scaled up by 10 %, respectively to match the same  $[\text{ap}] \cdot [\text{O}_3]$  levels as in (c). We attribute the strong increase of certain HOMs with low O:C ratios in (d) (red marker symbols) to a more efficient charging process with nitrate ions in our ion source due to assistance of water molecules rather than to an increased production inside the CLOUD chamber.

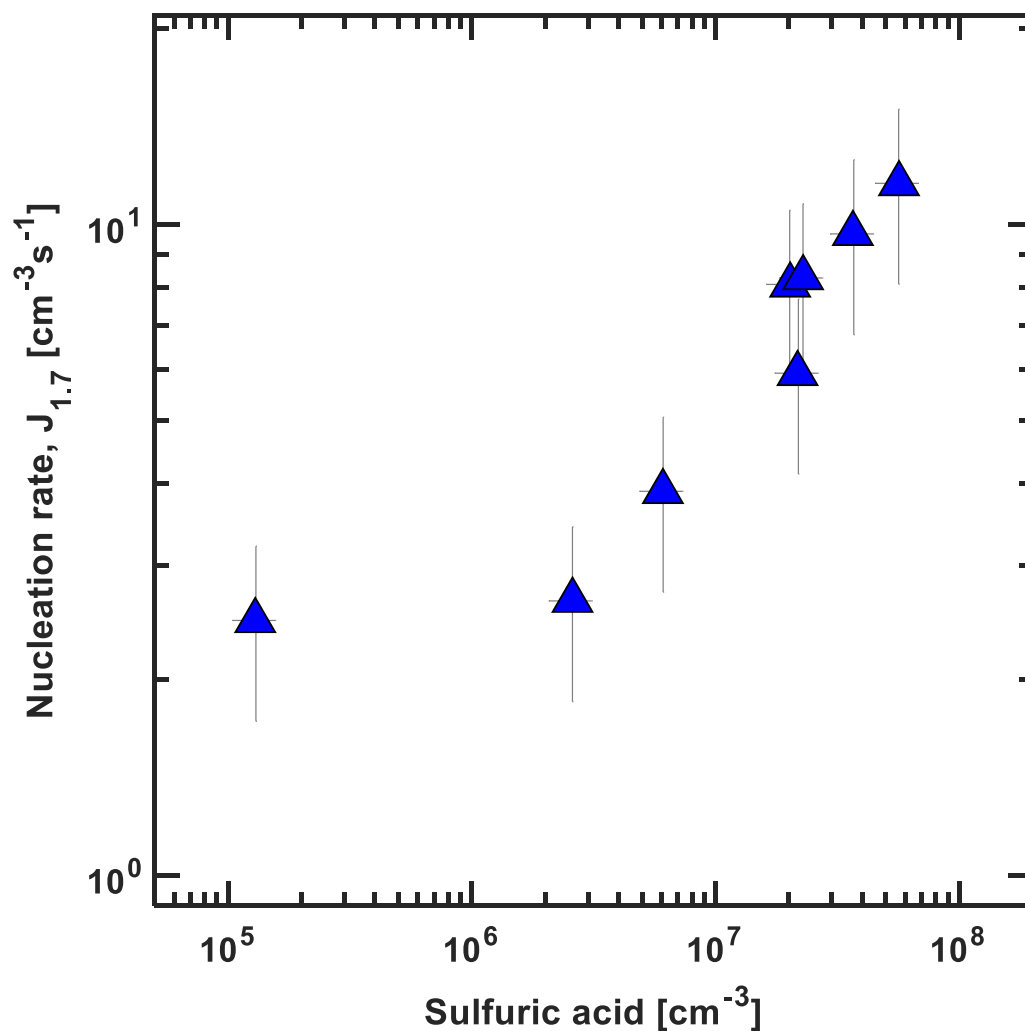


**Figure S8: Nucleation rate  $J_{1,7}$  (gr) vs sulfuric acid at +25 °C.**  $\alpha$ -pinene and isoprene levels were kept constant for all data points (around 1300 pptv and 4.5 ppbv, respectively), ozone levels ranged from 35 to 39 ppbv. HOM levels were fairly constant for all data points, ranging from  $1.2 \cdot 10^8$  to  $1.5 \cdot 10^8$  cm<sup>-3</sup>. All data was taken with excess ammonia (0.4 -2.5 ppbv), relative humidity was 38 % for all runs. Bars indicate 1 $\sigma$  run-to-run uncertainty. The overall systematic scale uncertainty of  $J$  for  $\pm 47$  % is not shown.

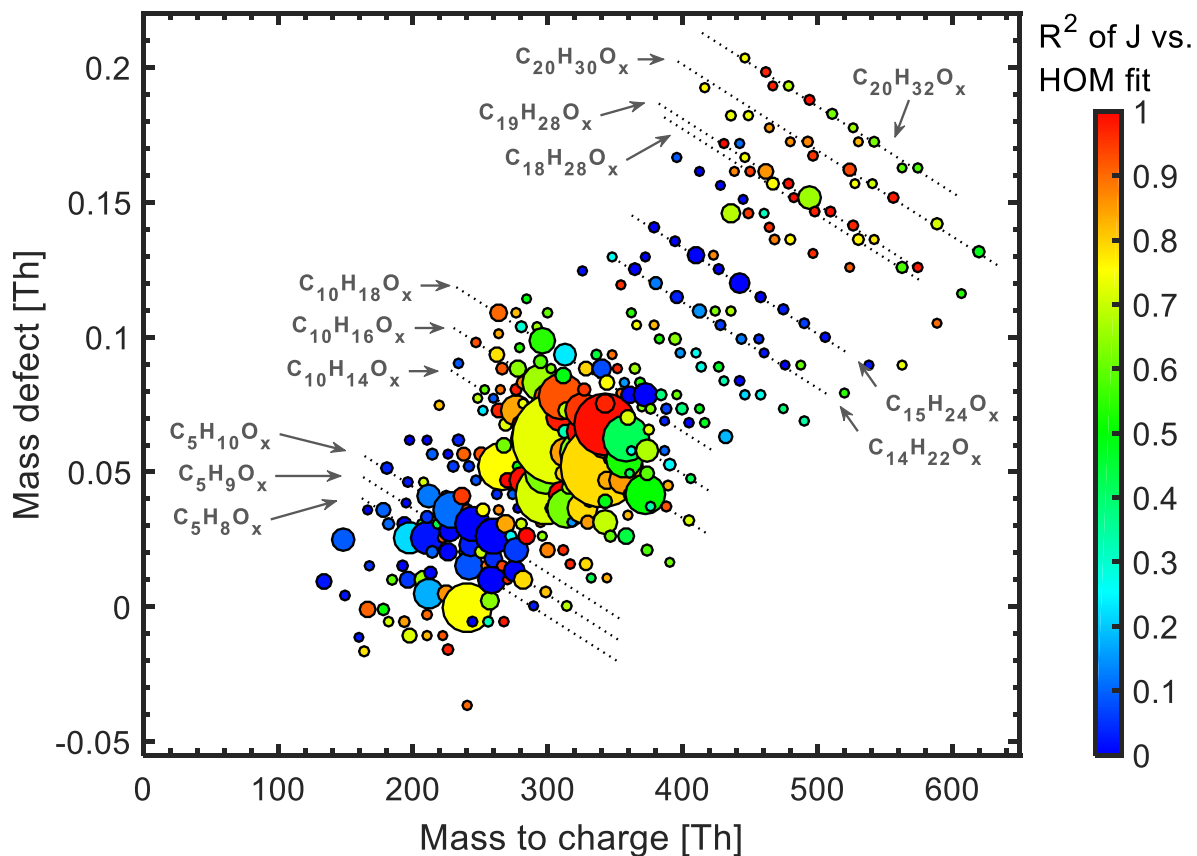


**Figure S9: Correlation of individual HOMs with nucleation rate  $J_{L,7}$ .** The data points displayed are taken from a run with 2.6 ppbv  $\alpha$ -pinene, 9.8 ppbv isoprene and 38 ppbv ozone under UV illuminated conditions. The area of the marker points is linearly scaled to the intensity of the HOM signals. The color code indicates coefficient of determination ( $R^2$ ) of a power law fit of  $J$  vs every individual HOM peak. The dataset used for the fit contains the six  $J_{ger}$  data points taken under low/medium/high  $\alpha$ -pinene levels with and without isoprene at +25 °C. High  $R^2$  does not necessarily mean that the corresponding molecules contribute directly to nucleation, but that they are predominantly formed in a chemical setting that favors the production of nucleator molecules.

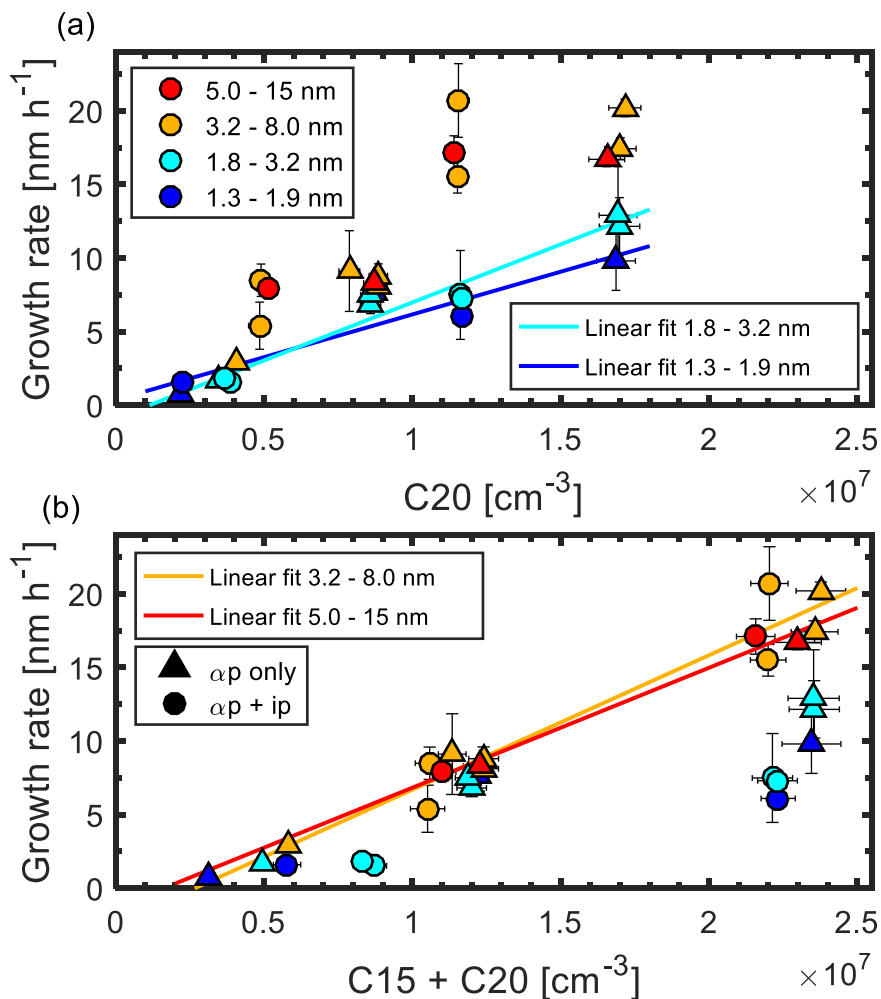


**Figure S10: Growth rate vs (a)  $C_{20}$  class concentration and (b)  $C_{15} + C_{20}$  class concentration at +5 °C and 38 % RH.** Growth rates were measured by scanning PSM (1.3 – 1.9 nm, dark blue), DMA-train (1.8 – 3.2 nm, light blue and 3.2 – 8.0 nm, orange) and nanoSMPS (5.0 – 15 nm, red). Triangles represent  $\alpha$ -pinene only runs, circles represent  $\alpha$ -pinene + isoprene runs. The growth rate between 1.8 nm and 3.2 nm can be parametrized by a linear fit when plotted against  $C_{20}$  class molecules, for the size range from 3.2 nm – 8.0 nm there is a linear relationship for growth rate when plotted against  $C_{15} + C_{20}$  class molecules.

## SI References

- Atkinson, R.: Gas-phase tropospheric chemistry of volatile organic compounds: 1. Alkanes and alkenes, *Journal of Physical and Chemical Reference Data*, 26, 215-290, 1997.
- Berndt, T., Richters, S., Kaethner, R., Voigtländer, J., Stratmann, F., Sipilä, M., Kulmala, M., and Herrmann, H.: Gas-Phase Ozonolysis of Cycloalkenes: Formation of Highly Oxidized RO<sub>2</sub> Radicals and Their Reactions with NO, NO<sub>2</sub>, SO<sub>2</sub>, and Other RO<sub>2</sub> Radicals, *The Journal of Physical Chemistry A*, 119, 10336-10348, 10.1021/acs.jpca.5b07295, 2015.
- Berndt, T., Richters, S., Jokinen, T., Hyttinen, N., Kurtén, T., Otkjær, R. V., Kjaergaard, H. G., Stratmann, F., Herrmann, H., Sipilä, M., Kulmala, M., and Ehn, M.: Hydroxyl radical-induced formation of highly oxidized organic compounds, *Nature Communications*, 7, 13677, 2016.
- Berndt, T., Mentler, B., Scholz, W., Fischer, L., Herrmann, H., Kulmala, M., and Hansel, A.: Accretion Product Formation from Ozonolysis and OH Radical Reaction of  $\alpha$ -Pinene: Mechanistic Insight and the Influence of Isoprene and Ethylene, *Environmental science & technology*, 2018.
- Bernhammer, A.-K., Fischer, L., Mentler, B., Heinritzi, M., Simon, M., and Hansel, A.: Production of highly oxygenated organic molecules (HOMs) from trace contaminants during isoprene oxidation, *Atmospheric Measurement Techniques*, 11, 4763-4773, 2018.
- Bernhammer, A. K., Breitenlechner, M., Keutsch, F. N., and Hansel, A.: Technical note: Conversion of isoprene hydroxy hydroperoxides (ISOPOOHs) on metal environmental simulation chamber walls, *Atmos. Chem. Phys.*, 17, 4053-4062, 10.5194/acp-17-4053-2017, 2017.
- Breitenlechner, M., Fischer, L., Hainer, M., Heinritzi, M., Curtius, J., and Hansel, A.: PTR3: An Instrument for Studying the Lifecycle of Reactive Organic Carbon in the Atmosphere, *Analytical Chemistry*, 89, 5824-5831, 10.1021/acs.analchem.6b05110, 2017.
- Duplissy, J., Merikanto, J., Franchin, A., Tsagkogeorgas, G., Kangasluoma, J., Wimmer, D., Vuollekoski, H., Schobesberger, S., Lehtipalo, K., Flagan, R. C., Brus, D., Donahue, N. M., Vehkamäki, H., Almeida, J., Amorim, A., Barmet, P., Bianchi, F., Breitenlechner, M., Dunne, E. M., Guida, R., Henschel, H., Junninen, H., Kirkby, J., Kürten, A., Kupc, A., Määttänen, A., Makhmutov, V., Mathot, S., Nieminen, T., Onnela, A., Praplan, A. P., Riccobono, F., Rondo, L., Steiner, G., Tome, A., Walther, H., Baltensperger, U., Carslaw, K. S., Dommen, J., Hansel, A., Petäjä, T., Sipilä, M., Stratmann, F., Vrtala, A., Wagner, P. E., Worsnop, D. R., Curtius, J., and Kulmala, M.: Effect of ions on sulfuric acid-water binary particle formation: 2. Experimental data and comparison with QC-normalized classical nucleation theory, *Journal of Geophysical Research: Atmospheres*, 121, 1752-1775, 10.1002/2015JD023539, 2016.
- Ehn, M., Thornton, J. A., Kleist, E., Sipilä, M., Junninen, H., Pullinen, I., Springer, M., Rubach, F., Tillmann, R., Lee, B., Lopez-Hilfiker, F., Andres, S., Acir, I.-H., Rissanen, M., Jokinen, T., Schobesberger, S., Kangasluoma, J., Kontkanen, J., Nieminen, T., Kurten, T., Nielsen, L. B., Jorgensen, S., Kjaergaard, H. G., Canagaratna, M., Maso, M. D., Berndt, T., Petaja, T., Wahner, A., Kerminen, V.-M., Kulmala, M., Worsnop, D. R., Wildt, J., and Mentel, T. F.: A large source of low-volatility secondary organic aerosol, *Nature*, 506, 476-479, 10.1038/nature13032, 2014.
- Eisele, F. L., and Tanner, D. J.: Measurement of the gas phase concentration of H<sub>2</sub>SO<sub>4</sub> and methane sulfonic acid and estimates of H<sub>2</sub>SO<sub>4</sub> production and loss in the atmosphere, *Journal of Geophysical Research: Atmospheres*, 98, 9001-9010, 10.1029/93JD00031, 1993.
- Elshorbany, Y. F., Kleffmann, J., Hofzumahaus, A., Kurtenbach, R., Wiesen, P., Brauers, T., Bohn, B., Dorn, H. P., Fuchs, H., and Holland, F.: HO<sub>x</sub> budgets during HO<sub>x</sub>Comp: A case study of HO<sub>x</sub> chemistry under NO<sub>x</sub>-limited conditions, *Journal of Geophysical Research: Atmospheres*, 117, 2012.
- Finlayson-Pitts, B. J., and Pitts Jr, J. N.: *Chemistry of the upper and lower atmosphere: theory, experiments, and applications*, Elsevier, 1999.

- Heinritzi, M., Simon, M., Steiner, G., Wagner, A. C., Kürten, A., Hansel, A., and Curtius, J.: Characterization of the mass-dependent transmission efficiency of a CIMS, *Atmos. Meas. Tech.*, 9, 1449-1460, 10.5194/amt-9-1449-2016, 2016.
- Hyttinen, N., Rissanen, M. P., and Kurtén, T.: Computational Comparison of Acetate and Nitrate Chemical Ionization of Highly Oxidized Cyclohexene Ozonolysis Intermediates and Products, *The Journal of Physical Chemistry A*, 121, 2172-2179, 10.1021/acs.jpca.6b12654, 2017.
- Kangasluoma, J., Kuang, C., Wimmer, D., Rissanen, M. P., Lehtipalo, K., Ehn, M., Worsnop, D. R., Wang, J., Kulmala, M., and Petäjä, T.: Sub-3 nm particle size and composition dependent response of a nano-CPC battery, *Atmos. Meas. Tech.*, 7, 689-700, 10.5194/amt-7-689-2014, 2014.
- Kirkby, J., Curtius, J., Almeida, J., Dunne, E., Duplissy, J., Ehrhart, S., Franchin, A., Gagné, S., Ickes, L., Kürten, A., Kupc, A., Metzger, A., Riccobono, F., Rondo, L., Schobesberger, S., Tsagkogeorgas, G., Wimmer, D., Amorim, A., Bianchi, F., Breitenlechner, M., David, A., Dommen, J., Downard, A., Ehn, M., Flagan, R. C., Haider, S., Hansel, A., Hauser, D., Jud, W., Junninen, H., Kreissl, F., Kvashin, A., Laaksonen, A., Lehtipalo, K., Lima, J., Lovejoy, E. R., Makhmutov, V., Mathot, S., Mikkilä, J., Minginette, P., Mogo, S., Nieminen, T., Onnela, A., Pereira, P., Petäjä, T., Schnitzhofer, R., Seinfeld, J. H., Sipilä, M., Stozhkov, Y., Stratmann, F., Tomé, A., Vanhanen, J., Viisanen, Y., Vrtala, A., Wagner, P. E., Walther, H., Weingartner, E., Wex, H., Winkler, P. M., Carslaw, K. S., Worsnop, D. R., Baltensperger, U., and Kulmala, M.: Role of sulphuric acid, ammonia and galactic cosmic rays in atmospheric aerosol nucleation, *Nature*, 476, 429, 10.1038/nature10343 2011.
- Kirkby, J., Duplissy, J., Sengupta, K., Frege, C., Gordon, H., Williamson, C., Heinritzi, M., Simon, M., Yan, C., Almeida, J., Tröstl, J., Nieminen, T., Ortega, I. K., Wagner, R., Adamov, A., Amorim, A., Bernhammer, A.-K., Bianchi, F., Breitenlechner, M., Brilke, S., Chen, X., Craven, J., Dias, A., Ehrhart, S., Flagan, R. C., Franchin, A., Fuchs, C., Guida, R., Hakala, J., Hoyle, C. R., Jokinen, T., Junninen, H., Kangasluoma, J., Kim, J., Krapf, M., Kürten, A., Laaksonen, A., Lehtipalo, K., Makhmutov, V., Mathot, S., Molteni, U., Onnela, A., Peräkylä, O., Piel, F., Petäjä, T., Praplan, A. P., Pringle, K., Rap, A., Richards, N. A. D., Riipinen, I., Rissanen, M. P., Rondo, L., Sarnela, N., Schobesberger, S., Scott, C. E., Seinfeld, J. H., Sipilä, M., Steiner, G., Stozhkov, Y., Stratmann, F., Tomé, A., Virtanen, A., Vogel, A. L., Wagner, A. C., Wagner, P. E., Weingartner, E., Wimmer, D., Winkler, P. M., Ye, P., Zhang, X., Hansel, A., Dommen, J., Donahue, N. M., Worsnop, D. R., Baltensperger, U., Kulmala, M., Carslaw, K. S., and Curtius, J.: Ion-induced nucleation of pure biogenic particles, *Nature*, 533, 521-526, 10.1038/nature17953, 2016.
- Kroll Jesse, H., Hanisco Thomas, F., Donahue Neil, M., Demerjian Kenneth, L., and Anderson James, G.: Accurate, direct measurements of OH yields from gas-phase ozone-alkene reactions using an in situ LIF Instrument, *Geophysical Research Letters*, 28, 3863-3866, 10.1029/2001GL013406, 2001.
- Kulmala, M., Kontkanen, J., Junninen, H., Lehtipalo, K., Manninen, H. E., Nieminen, T., Petäjä, T., Sipilä, M., Schobesberger, S., Rantala, P., Franchin, A., Jokinen, T., Järvinen, E., Äijälä, M., Kangasluoma, J., Hakala, J., Aalto, P. P., Paasonen, P., Mikkilä, J., Vanhanen, J., Aalto, J., Hakola, H., Makkonen, U., Ruuskanen, T., Mauldin, R. L., Duplissy, J., Vehkamäki, H., Bäck, J., Kortelainen, A., Riipinen, I., Kurtén, T., Johnston, M. V., Smith, J. N., Ehn, M., Mentel, T. F., Lehtinen, K. E. J., Laaksonen, A., Kerminen, V.-M., and Worsnop, D. R.: Direct Observations of Atmospheric Aerosol Nucleation, *Science*, 339, 943-946, 10.1126/science.1227385, 2013.
- Kürten, A., Rondo, L., Ehrhart, S., and Curtius, J.: Performance of a corona ion source for measurement of sulfuric acid by chemical ionization mass spectrometry, *Atmos. Meas. Tech.*, 4, 437-443, 10.5194/amt-4-437-2011, 2011.
- Kürten, A., Rondo, L., Ehrhart, S., and Curtius, J.: Calibration of a Chemical Ionization Mass Spectrometer for the Measurement of Gaseous Sulfuric Acid, *The Journal of Physical Chemistry A*, 116, 6375-6386, 10.1021/jp212123n, 2012.
- Kürten, A., Bergen, A., Heinritzi, M., Leiminger, M., Lorenz, V., Piel, F., Simon, M., Sitals, R., Wagner, A. C., and Curtius, J.: Observation of new particle formation and measurement of sulfuric acid, ammonia, amines and highly oxidized organic molecules at a rural site in central Germany, *Atmospheric Chemistry and Physics*, 16, 12793-12813, 2016.

- Lee, S.-H., Uin, J., Guenther, A. B., de Gouw, J. A., Yu, F., Nadykto, A. B., Herb, J., Ng, N. L., Koss, A., Brune, W. H., Baumann, K., Kanawade, V. P., Keutsch, F. N., Nenes, A., Olsen, K., Goldstein, A., and Ouyang, Q.: Isoprene suppression of new particle formation: Potential mechanisms and implications, *Journal of Geophysical Research: Atmospheres*, 121, 14,621-614,635, 10.1002/2016JD024844, 2016.
- Lehtipalo, K., Leppä, J., Kontkanen, J., Kangasluoma, J., Franchin, A., Wimmer, D., Schobesberger, S., Junninen, H., Petäjä, T., Sipilä, M., Mikkilä, J., Vanhanen, J., Worsnop, D. R., and Kulmala, M.: Methods for determining particle size distribution and growth rates between 1 and 3 nm using the Particle Size Magnifier, *Boreal Env. Res.*, 19 (suppl. B), 215-236, 2014.
- Lelieveld, J., Gromov, S., Pozzer, A., and Taraborrelli, D.: Global tropospheric hydroxyl distribution, budget and reactivity, *Atmos. Chem. Phys.*, 16, 12477-12493, 10.5194/acp-16-12477-2016, 2016.
- Madronich, S., and Calvert, J. G.: Permutation reactions of organic peroxy radicals in the troposphere, *Journal of Geophysical Research: Atmospheres*, 95, 5697-5715, 1990.
- Malkin, T. L., Goddard, A., Heard, D. E., and Seakins, P. W.: Measurements of OH and HO<sub>2</sub> yields from the gas phase ozonolysis of isoprene, *Atmos. Chem. Phys.*, 10, 1441-1459, 10.5194/acp-10-1441-2010, 2010.
- Martinez, M., Harder, H., Kubistin, D., Rudolf, M., Bozem, H., Eerdeken, G., Fischer, H., Klüpfel, T., Gurk, C., Königstedt, R., Parchatka, U., Schiller, C. L., Stickler, A., Williams, J., and Lelieveld, J.: Hydroxyl radicals in the tropical troposphere over the Suriname rainforest: airborne measurements, *Atmos. Chem. Phys.*, 10, 3759-3773, 10.5194/acp-10-3759-2010, 2010.
- Massoli, P., Stark, H., Canagaratna, M. R., Krechmer, J. E., Xu, L., Ng, N. L., Mauldin III, R. L., Yan, C., Kimmel, J., and Misztal, P. K.: Ambient Measurements of Highly Oxidized Gas-Phase Molecules during the Southern Oxidant and Aerosol Study (SOAS) 2013, *ACS Earth and Space Chemistry*, 2, 653-672, 2018.
- Seinfeld, J. H., and Pandis, S. N.: *Atmospheric chemistry and physics: from air pollution to climate change*, John Wiley & Sons, 2016.
- Stevens, P., Mather, J., Brune, W. H., Eisele, F., Tanner, D., Jefferson, A., Cantrell, C., Shetter, R., Sewall, S., and Fried, A.: HO<sub>2</sub>/OH and RO<sub>2</sub>/HO<sub>2</sub> ratios during the Tropospheric OH Photochemistry Experiment: Measurement and theory, *Journal of Geophysical Research: Atmospheres*, 102, 6379-6391, 1997.
- Stolzenburg, D., Steiner, G., and Winkler, P. M.: A DMA-train for precision measurement of sub-10 nm aerosol dynamics, *Atmos. Meas. Tech.*, 10, 1639-1651, 10.5194/amt-10-1639-2017, 2017.
- Taraborrelli, D., Lawrence, M. G., Crowley, J. N., Dillon, T. J., Gromov, S., Groß, C. B. M., Vereecken, L., and Lelieveld, J.: Hydroxyl radical buffered by isoprene oxidation over tropical forests, *Nature Geoscience*, 5, 190, 10.1038/ngeo1405 2012.
- Tillmann, R., Hallquist, M., Jonsson, Å. M., Kiendler-Scharr, A., Saathoff, H., Iinuma, Y., and Mentel, T. F.: Influence of relative humidity and temperature on the production of pinonaldehyde and OH radicals from the ozonolysis of  $\alpha$ -pinene, *Atmos. Chem. Phys.*, 10, 7057-7072, 10.5194/acp-10-7057-2010, 2010.
- Vanhanen, J., Mikkilä, J., Lehtipalo, K., Sipilä, M., Manninen, H. E., Siivola, E., Petäjä, T., and Kulmala, M.: Particle Size Magnifier for Nano-CN Detection, *Aerosol Science and Technology*, 45, 533-542, 10.1080/02786826.2010.547889, 2011.
- Wallington, T., Dagaut, P., and Kurylo, M.: UV absorption cross sections and reaction kinetics and mechanisms for peroxy radicals in the gas phase, *Chemical reviews*, 92, 667-710, 1992.
- Yan, C., Nie, W., Äijälä, M., Rissanen, M. P., Canagaratna, M. R., Massoli, P., Junninen, H., Jokinen, T., Sarnela, N., and Häme, S. A.: Source characterization of highly oxidized multifunctional compounds in a boreal forest environment using positive matrix factorization, *Atmospheric Chemistry and Physics*, 16, 12715-12731, 2016.